Aqueous Ion Transport Properties and Water Reorientation Dynamics from Ambient to Supercritical Conditions

Perla B. Balbuena,[†,§] Keith P. Johnston,[*,†] Peter J. Rossky,[‡] and Jin-Kee Hyun[†,‡]

Department of Chemical Engineering and Department of Chemistry and Biochemistry, The University of Texas at Austin Austin, Texas 78712

Received: September 3, 1997; In Final Form: February 5, 1998

Ion transport properties including the friction coefficient, Walden product (product of conductivity and viscosity), and the limiting equivalent conductance are predicted in water at elevated temperatures using a semicontinuum model. Molecular dynamics computer simulation is used to determine water rotational reorientation times in the first coordination shell compared with the bulk, and the results are incorporated into a hydrodynamic expression for the ionic friction coefficient. Along the coexistence curve of water, the effective Stokes−Einstein radius implied by the model is relatively constant. However, for Cl^-, K^+, and Rb^+, this radius increases at typical supercritical water conditions, where the motion of the first shell water molecules is coupled more closely to that of the ion. For Na^+, the coupling is already quite strong at higher solvent densities. The increment to the friction coefficient in excess of the bare ion Stokes−Einstein result contributes a larger fraction of the total in supercritical water at typical densities (up to 0.29 g/cm^3) than it does in higher density subcritical water, as a result of electrostriction. The limiting equivalent conductance increases approximately linearly with decreasing solvent density in the supercritical regime, in qualitative accord with the experimental extrapolations of Quist and Marshall (*J. Phys. Chem.* **1968**, *72*, 684−703) and in contrast to the plateau with decreasing density inferred from much more recent experiments by Zimmerman *et al.* (*J. Phys. Chem.* **1995**, *99*, 11612−11625).

Introduction

Ion transport in supercritical water (SCW) solutions may be characterized by measuring diffusion coefficients, conductivities, and viscosities either experimentally or by computer simulations. Despite the importance of these properties to chemical kinetics and separation processes and as indicators of speciation, remarkably few studies have been reported for solutes in SCW solutions. Traditionally, most of the experimental equilibrium association constants for acids, bases, and salts in SCW have been inferred from conductivity measurements by utilizing transport models to extrapolate conductivity data to infinite dilution.[1,2] In pure SCW, diffusion constants have been measured by NMR spin−echo techniques by Lamb et al.[3] The Stokes−Einstein equation that relates diffusive and viscous flows has been widely used to correlate an effective radius empirically.[4,5] Although this empirical approach is of value for correlating experiments, it is limited in terms of mechanistic analysis and predictive capacity.

In SCW, ion solvation is much stronger than expected on the basis of the bulk dielectric constant. According to molecular dynamics simulation, extreme conditions (e.g., reduced densities of 0.05 and 0.3 for reduced temperatures of 1.0 and 1.3, respectively) are necessary to remove half of the water molecules in the first solvation shell about the chloride ion.[6] By analogy to adsorption phenomena, augmentation in the local solvent density relative to the bulk can be modeled quite effectively with a Langmuir isotherm.[7] This local density augmentation is sometimes termed solvent−solute clustering or microheterogeneous solvation; for ionic solutes, the term electrostriction is also used. Electrostriction has a large effect on the free energy of ion solvation,[8] the equilibrium and rate constants for chemical reactions,[9,10,] and on ion pairing.[11] Solvent−solute clustering has a much larger effect on the free energy of solvation of ions relative to nonelectrolytes because of the stronger solute−solvent interaction[10] and may be expected to have a strong influence on ion transport.

Molecular dynamics (MD) simulations have been used to study diffusion in pure SCW. Self-diffusion coefficients have been evaluated,[12,13] but for important solutes, there is a general lack of theoretical information by which one can develop insight and principles. Recently, we have begun an effort to understand the details of the dynamics of ion−water interactions in SCW by analyzing[6] the residence time of molecules in the solvation shell of ions. In SCW, lifetimes were only four times shorter than in ambient water, despite the large change in structure and temperature.

Our present objective is to evaluate friction coefficients of ions in aqueous solutions at infinite dilution via a semicontinuum hydrodynamic model.[14] The molecular part of the model utilizes MD simulation to incorporate local friction present in the first coordination shell. The local friction is expressed in terms of the rotational reorientation times for water about a central water molecule compared with that about a central ion. One expects that this relative time is correlated with the degree to which the ionic motion can be described as diffusion of the ion and its hydration shell as a unit, or, in the other extreme, diffusion of the bare ion relative to the bulk solvent. After discussing the rotational reorientation times, we analyze the Walden product

* To whom correspondence should be addressed.
† Department of Chemical Engineering.
‡ Department of Chemistry and Biochemistry.
§ Present address: Department of Chemical Engineering, University of South Carolina, Columbia, South Carolina 29208.

S1089-5647(97)02870-8 CCC: $15.00
Published on Web 04/22/1998

(product of conductivity and viscosity), the effective Stokes radius, and the so-called residual friction, defined as the difference between the total friction and the Stokes−Einstein friction determined for the bare ion radius. The results for the residual friction are interpreted in terms of the ionic coordination number. Emphasis is placed on contrasting the behavior in SCW where solvent densities are still relatively high and SCW where densities are typically lower by an order of magnitude or more. We emphasize values no more than 0.29 g/cm^3, a density range rather typical for experimental studies of SCW; few studies examine higher densities because these densities require extreme pressures. The final section compares our predictions with conductivity experiments and attempts to clarify inconsistencies between alternative data sets[1,2] with regard to the behavior at low solvent density.

Semicontinuum Model for Limiting Ionic Conductances

The semicontinuum model used here is based on that first proposed by Impey *et al.*[14] for the calculation of Walden products in aqueous ionic solutions at ambient conditions. It is based on an approximate expression for the friction coefficient experienced by an ion, from which the transport coefficients follow immediately. The friction coefficient expression follows from an approximate solution to the Navier−Stokes equation.[15] In the creeping flow regime, where inertial terms can be neglected, the Navier−Stokes equation can be written in terms of the fluid velocity **v** and pressure P as:

$$\nabla\cdot(\eta(\mathbf{r})\nabla\mathbf{v}) = \nabla P \tag{1}$$

When the viscosity is a constant, the solution to this equation for the friction on an impenetrable sphere leads to the well-known Stokes−Einstein equation[15] $\zeta = \sigma\pi\eta R$, where ζ is the friction coefficient, σ is a constant (varying for this case with boundary conditions), η is the bulk viscosity, and R is the ionic radius. The parameter ζ is simply related to the diffusion constant D via the Stokes−Einstein relation $\zeta = kT/D$ where k is Boltzmann's constant and T is the temperature.

The resulting velocity profile is usually expressed in terms of a convenient two-dimensional flow representation known as stream function ψ that automatically satisfies the continuity equation. In polar coordinates (r, α), the stream function and pressure of the fluid surrounding the sphere have the following form:[15,16]

$$\psi = U_\infty a(r) \sin^2 \alpha$$

$$P = P_\infty - U_\infty \eta b(r) \cos \alpha \tag{2}$$

where *a(r)* and *b(r)* are known functions of the radial distance and the radius of the sphere,[15,16] and U_∞ and P_∞ are the bulk velocity and pressure, respectively.

For a fluid of varying viscosity, Brilliantov and Krapinsky[16] have solved eq 1 assuming that the stream function and pressure profiles have similar form to eqs 2, with *unknown* functions *a(r)* and *b(r)*. This assumption yields a generalized friction coefficient in terms of *a(r)* and *b(r)*.[16] The final form of these functions can be obtained applying boundary conditions for the velocity and pressure at the surface of the sphere and at distances far enough where bulk conditions hold. When the viscosity varies with radius, two particular choices of *b(r)* lead to a solution for the friction coefficient of the form

$$\frac{1}{\zeta} = \int_{R_I}^{\infty} \frac{dr}{\sigma\pi r^2 \eta(r)} \tag{3}$$

For a constant pressure [i.e., $b(r) = 0$] $\sigma = 4$. For another approximate value of the pressure field, assuming that $b(r) = b_o(r)$, where $b_o(r)$ describes the pressure profile resulting from the assumption of *constant* viscosity, they obtain 6 in place of 4 for σ. It should be noted that Brilliantov and Krapinsky have used stick boundary conditions at the sphere surface to obtain these expressions for the friction coefficient, and the two different values of σ have been obtained depending on the expression for the pressure field, rather than on the boundary conditions. Earlier, Wolynes[17] solved eq 1 with a constant pressure using an approximation termed "pre-angular averaging". As a result, he also obtained $\sigma = 4$. Note that in both formulations, the value of σ is not an immediate reflection of the surface boundary conditions, despite the apparent equivalence to the stick and slip boundary condition solutions for Stokes law. We also note that the time dependence of polarization described in previous models[18,19] is not explicitly included in eq 3, but the effect is implicit in η(r). Later, we will consider both of the values $\sigma = 4$ and $\sigma = 6$ in eq 3, but for the major part of this work, we emphasize $\sigma = 4$, corresponding to the development of Impey et al.[14] based on the work of Wolynes.[17]

The present semicontinuum model is based on the use of eq 3 for an ion of radius R_I diffusing in a medium of nonuniform viscosity. It is assumed here that the solvent viscosity can be described by a step profile:

$$\eta(r) = \eta_{bulk} \equiv \eta \qquad \text{for } r > R_C$$

$$\eta(r) = \eta_S \qquad \text{for } r < R_C \tag{4}$$

where R_C is the radius of an ion−water complex that includes the first shell of water molecules surrounding the ion, and η_s is the viscosity in this shell. Integrating eq 3 with the viscosity profile given by eq 4, the friction coefficient becomes

$$\frac{1}{\zeta} = \frac{1}{\sigma\pi\eta R_I}\left\{\frac{\eta}{\eta_S} + \frac{R_I}{R_C}\left(1 - \frac{\eta}{\eta_S}\right)\right\} \tag{5}$$

Equation 5 reduces to a Stokes−Einstein friction coefficient form, with ζ proportional to ηR, with a radius $R = R_I$ when $\eta = \eta_s$ and with a radius R_c, when η/η_s is equal to zero (η_s very large). For ambient conditions, it was determined[14] that η/η_s had an intermediate value.

A method is needed to define the viscosity of the water molecules in the first shell of the ion. Following Impey et al.,[14] η and η_s may be related to characteristic dipole reorientation times for water molecules in the first shell about (1) a central water molecule (τ^R_{bulk}) and (2) an ion (τ^R_{ion}) via the continuum relations for rotational diffusion of a sphere with stick boundary conditions. That is,

$$\tau^R_{ion} = \frac{8\pi\eta_S R^3}{kT} \tag{6}$$

and

$$\tau^R_{bulk} = \frac{8\pi\eta R^3}{kT} \tag{7}$$

where R is the radius of the sphere. Several nuclear magnetic relaxation (NMR) studies in pure water[20] have shown that eq 7, known as the Debye equation, describes very well reorientation of water at subcritical conditions. From MD simulations, one can obtain characteristic reorientation times from the time-

correlation function (TCF):

$$c_l(t) = \langle P_l(u_i(t + t_o)\cdot \underline{u}_i(t_o))\rangle_{t_o} \quad (8)$$

where $\underline{u}_i$ is a unit vector that characterizes the orientation of molecule i, P_l is the Legendre polynomial of degree l, and the average is over many initial times t_o.

Several choices can be made for $\underline{u}_i$, such as the direction of the water dipole or the direction of the OH bond, and in favorable cases, these TCFs can be directly related to spectral band shapes.[21] In this work, we use for $\underline{u}_i$ the unit vector in the direction of the water dipole characterized by the angle θ between the vector from the oxygen of the water to the center of the ion and the direction of the water dipole. We define the correlation time via the $l = 1$ function, and the bulk and shell rotational reorientation times are calculated from

$$\tau = \int_0^\infty c(t)\, dt \quad (9)$$

In some cases, in particular for small monovalent and bivalent cations at low temperatures where the simulation run was not long enough to determine the full decay of $c(t)$, the MD result was extrapolated by an exponential function that best described the decay in the region between 3 and 6 ps, as in previous studies.[22] However, because the majority of the state points considered in this study are at relatively high temperatures, the reorientation times were determined from full simulation results in most cases.

Substituting eqs 6 and 7 into eq 5, the friction coefficient is thus calculated from

$$\frac{1}{\zeta} = \frac{1}{\sigma\pi\eta R_I}\left\{\frac{\tau^R_{bulk}}{\tau^R_{ion}} + \frac{R_I}{R_C}\left(1 - \frac{\tau^R_{bulk}}{\tau^R_{ion}}\right)\right\} \quad (10)$$

By comparing this result with the Stokes−Einstein form, an effective Stokes radius may be defined as

$$R_{eff} = R_I\left\{\frac{\tau^R_{bulk}}{\tau^R_{ion}} + \frac{R_I}{R_C}\left(1 - \frac{\tau^R_{bulk}}{\tau^R_{ion}}\right)\right\}^{-1} \quad (11)$$

Equation 18 makes clear one advantage of this approach for studying transport properties; that is, only the *ratio* of reorientation times appears, and this may be expected to be less dependent than the individual times on errors due to the specific form of the potential functions. Given the friction coefficient, it is straightforward to determine the limiting ionic conductance $\Lambda_o = Fe/\zeta$, diffusion coefficient $D = kT/\zeta$, and the product of limiting conductance times viscosity, or Walden product

$$\Lambda_o\eta = Fe/(\zeta/\eta) \quad (12)$$

where F is the Faraday constant and e is the electron charge. Thus, given ζ, only bulk properties are required to determine each of these transport properties. We note that at a given T, the diffusion coefficient is simply proportional to Λ_o.

Method

The MD simulations were performed for one ion and 500 SPC/E[23] water molecules. Periodic boundary conditions were imposed and the long-range interactions were accounted for by Ewald summation.[24,25] The ion was kept in a fixed position and the dynamics of the water molecules was calculated. Similarly, for the simulations of pure water, one water molecule was kept in a fixed position, while the dynamics of the surrounding molecules was examined. State points were characterized on the basis of the corresponding densities for the SPC/E model as calculated by Guillot and Guissani.[26] At subcritical conditions, we considered state points on the saturation curve of liquid water, from ambient temperature to 300 °C. The viscosities of the bulk solvent were obtained from the NIST equation of state.[27]

TABLE 1: Reorientational Times ($l = 1$) for Dipoles in the First Coordination Shell (see text) of Pure Water, for Conditions Along the Coexistence Curve of Liquid Water and at Supercritical Conditions

T, K	ρ, g/cm^3	$10^2\,\eta$, g/cm s	τ^R_{bulk}, ps	run lengths, ps
298	0.997	0.8903	2.33 ± 0.23	100
373	0.958	0.2823	0.99 ± 0.13	40
473	0.850	0.1345	0.46 ± 0.04	40
573	0.670	0.0860	0.37 ± 0.05	40
673	0.5	0.0654	0.20 ± 0.04	240
673	0.4	0.0528	0.21 ± 0.03	240
673	0.29	0.0415	0.14 ± 0.04	200
673	0.087	0.0250	0.19 ± 0.03	200

The ion−water potential models and parameters used in the simulations are the same as described in our previous work (Table 1, ref 8). Error bars in the time correlation functions were calculated according to the following procedure: First, a standard deviation is calculated for each time t from:

$$\sigma(t) = \frac{1}{N_{IT}}\left[\sum_{t_i=1}^{t_i=N_{IT}} (c(t)|_{t_o = t_i} - \langle c(t)\rangle_{t_o})^2\right]^{1/2} \quad (13)$$

where the summation is over N_{IT} different initial times, and $\langle c(t)\rangle_{t_o}$ is the average over all N_{IT} initial times t_o. Once the standard deviation is calculated at each time, two new curves are constructed: $c(t) + \sigma(t)$ and $c(t) - \sigma(t)$, and corresponding characteristic times are obtained: $\tau_{c+\sigma}$, $\tau_{c-\sigma}$, resulting in an estimated error range around the average value of τ.

Results and Discussion

Characteristic Rotational Times. *Pure Water.* The correlation functions given by eq 8 (with $l = 1$) for pure water were calculated. The function $c_1(t)$ for AW yields a similar decay to the one reported for the TIP4P model.[28,29] The calculated reorientation times are given in Table 1 according to eq 9 with $l = 1$ for pure subcritical and supercritical water. The reorientation times in AW in Table 1 are intermediate between those calculated for other water models: TIP4P[30] (3.3 ps at 292 K) and ST2 (1.5 ps at 299 K).[31] Self-diffusion coefficients obtained by MD simulations[13] using the SPC/E rigid model are in excellent agreement with NMR measurements.[3]

To check the predicted temperature dependence of the calculated reorientation times, we have compared the calculated bulk reorientation times for water ($l = 1$ in eq 8) with the experimental NMR values ($l = 2$) from Jonas et al.[20] The decay of correlations with increasing temperature is very similar. For example, in going from 303 to 363 K, the reported experimental values are reduced by a factor of 0.41, which is comparable to the calculated reduction by a factor of 0.42 for the change from 298 to 373 K (see Table 1). Considering the fact, noted earlier, that we will focus on *ratios* of reorientation times, this agreement is satisfactory.

At 373 K, we note that the calculated correlations decay much faster, and the reorientation time is reduced more than half compared with AW (Table 1). At 473 K, the reorientation time is five times faster than in ambient conditions. The large change

TABLE 2: Reorientation Times of Dipoles ($l = 1$) in the First Coordination Shell ($r < R_C$) of Ions for Conditions Along the Coexistence Curve of Liquid Water and at Supercritical Conditions

T, K	ρ, g/cm^3	Na^+	K^+	Rb^+	Cl^-	run lengths, ps
298	0.997	11.5 ± 0.6	5.0 ± 0.5	3.6 ± 0.8	2.6 ± 0.2	100
373	0.958	7.1 ± 0.4	1.6 ± 0.1	1.6 ± 0.11	1.2 ± 0.07	40
473	0.850	2.24 ± 0.22	0.83 ± 0.06	0.92 ± 0.07	0.7 ± 0.06	40
573	0.670	1.31 ± 0.15	0.85 ± 0.11	0.63 ± 0.06	0.44 ± 0.04	40
673	0.29	1.07 ± 0.11	0.56 ± 0.06	0.56 ± 0.05	0.42 ± 0.05	200
673	0.087	0.99 ± 0.11	0.65 ± 0.07	0.60 ± 0.06	0.42 ± 0.04	200

TABLE 3: Ratios $\tau^R_{bulk}/\tau^R_{ion}$ for Subcritical Conditions Along the Coexistence Curve of Liquid Water and for Supercritical Conditions at 673 K

T, K	ρ, g/cm^3	Cl^-	Na^+	K^+	Rb^+
298	0.997	0.90 ± 0.15	0.20 ± 0.10	0.47 ± 0.10	0.65 ± 0.17
373	0.958	0.85 ± 0.15	0.14 ± 0.03	0.61 ± 0.11	0.62 ± 0.11
473	0.850	0.66 ± 0.12	0.20 ± 0.03	0.55 ± 0.09	0.5 ± 0.09
573	0.670	0.84 ± 0.17	0.28 ± 0.06	0.43 ± 0.10	0.58 ± 0.12
673	0.29	0.33 ± 0.12	0.13 ± 0.05	0.25 ± 0.10	0.25 ± 0.09
673	0.087	0.45 ± 0.09	0.19 ± 0.04	0.29 ± 0.01	0.32 ± 0.02

TABLE 4: Dynamic Properties at Various Supercritical Conditions in Addition to Those in Table 2 (T_r and ρ_r reduced by SPCE model values, $T_c = 640$ K, $\rho_c = 0.29$ g/cm^3, and $P_c = 160$ bar)[a]

ion	T_r	ρ_r	τ^r_{ion}, ps	$\tau^r_{bulk}/\tau^r_{ion}$
Cl^-	1.035	0.93*	0.46	0.54 ± 0.12
	1.040	0.81*	0.41	0.56 ± 0.14
	1.045	0.70*	0.45	0.42 ± 0.10
Na^+	1.035	0.93*	0.86	0.29 ± 0.07
	1.040	0.81*	0.96	0.24 ± 0.07
	1.045	0.70*	1.0	0.19 ± 0.04
	1.052	1.72	0.74	0.27 ± 0.07
	1.052	1.38	1.11	0.19 ± 0.08
Sr^{2+}	1.052	1.0	2.6	0.05
	1.052	0.3	0.97	0.19
Ca^{2+}	1.052	1.0	2.1	0.07
	1.052	0.3	1.44	0.13

[a] (*) Denotes simulations at 280 bar.

in dynamics could be viewed as consistent with the breakdown of the extended hydrogen bonded network of water, which has been inferred in simulations[26] and neutron scattering,[32] but the size of this change is not surprising. The size is completely consistent with that expected based on the temperature dependence around room temperature, with an Arrhenius-like behavior characterized by an activation energy of ~3 kcal/mol.

In SCW at the densities studied, the behavior is different. Rotational rates are increased substantially, but at very low densities, the decay is actually slower than at somewhat higher densities (Table 1). Because the coordination number in the first shell is similar at both densities,[8] the slower decay is reasonably attributed to a reduction in balancing interactions with water molecules beyond the first shell. With this reduction in balancing interactions, the first shell is coupled more strongly to a central water molecule. The manifestations of such effects were observed previously in MD simulations of pure SCW by Mizan et al.,[33] who found the lifetime of the water−water H-bonds to decrease with increasing density. On the average, rotational times in the first shell of SCW are about half the value of those on the saturation curve at 573 K and are smaller by an order of magnitude compared with AW conditions.

Ions at Infinite Dilution. The state points in Tables 2 and 3 were chosen to match our previous study of the structure and thermodynamic properties of ion solvation.[8] Additional state points are provided separately in Table 4 and were chosen to match the reduced conditions of experimental data discussed next.

At 298 K, the decay of the dipole correlation for water molecules in the first shell of ions varies significantly as a function of the ion charge and radius (Table 2). The smaller cation, Na^+, attracts water strongly, and the time correlation function (not shown) persists to ~40 ps, which is reflected in a long reorientation time. For the larger cation, K^+, the correlations decay more slowly than for the similar size anion Cl^- in the first 1 ps at low temperature, yielding a reorientation time near Cl^- that is about half the value for K^+ (Table 2). The difference becomes much smaller at elevated temperature. Also, the dipole correlation near Cl^- decays more slowly than that near another water in the first 3 ps, and somewhat faster thereafter, yielding very similar reorientation times for the two (see Tables 1 and 2), in agreement with experimental findings.[34,35] In AW, reorientation times are much longer for bivalent cations: 16.5 ps for Sr^{2+} and 46.5 ps for Ca^{2+}. These much longer times are consistent with the stronger Coulombic interactions between divalent cations and water.

As temperature increases and density decreases on the water coexistence curve, the reorientation times about ions decrease substantially (Table 2). The ratios of reorientation times are in qualitative agreement with those estimated from NMR measurements at the same conditions.[34,35] They decrease by a factor of ~6 from 298 to 573 K. However, the ratio $\tau^R_{bulk}/\tau^R_{ion}$ is relatively constant from 298 to 573 K despite the large changes in the individual reorientation times (Table 3). The small change in this ratio is perhaps surprising given the large increase in thermal energy and the expected degradation of the hydrogen bonding structure of pure water. However, the result simply reflects the fact that the rate of change with temperature of the two times is nearly the same in this relatively high-density regime. We note that at 573 K, the density is still 0.67 g/cm^3. If put in the context of an Arrenhius-like expression for the rates, the insensitivity to temperature dependence is a result of nearly equal activation energies for reorientation near the ion and in the bulk solvent. As already noted in the discussion of pure water, the temperature dependence of the rates does not vary strongly along the coexistence curve.

At typical SCW densities ($\rho \leq \rho_c$), compared with subcritical water, a rather different type of behavior is typically observed for the reorientation time ratios. The value of τ^R_{ion} continues to decrease as temperature increases. For Na^+, $C(t)$ is reduced by one-half in ~0.3 ps in SCW, yet this decay is 16 times slower (5 ps) in AW. For Cl^-, the decay is ~10 times slower in AW. Nevertheless, τ^R_{ion} typically decreases at a notably slower rate than τ^R_{bulk}. Consequently, $\tau^R_{bulk}/\tau^R_{ion}$ decays markedly, whereas it is relatively constant in subcritical water. For Na^+, the effect is masked by the fact that τ^R_{ion} is relatively larger in subcritical water than it is for the larger ions. For bivalent cations, such as Ca^{2+}, slow decays persist even at these elevated temperatures, as shown in Table 4, and, as for Na^+, the ratio $\tau^R_{bulk}/\tau^R_{ion}$ is small in both AW and SCW (cf. values in Tables 4 and 5).

The noted differences in behavior for $\tau^R_{bulk}/\tau^R_{ion}$ in subcritical versus supercritical water is easily understood in light of the aforementioned observations. The water density is much lower

TABLE 5: Walden Products for Ions in Aqueous Solutions at AW Conditions ($\sigma = 4$ in eq 10)

ion	R_I, Å	R_C, Å	$\tau^R_{bulk}/\tau^R_{ion}$	$\Lambda_o\eta$, calc, [S g cm/s] (eq 12)	$\Lambda_o\eta$, exp, [S g cm/s][43,44]
Cl^-	1.8	4.2	0.90	0.64	0.67−0.69
Na^+	0.9	3.5	0.20	0.56	0.45
K^+	1.4	3.9	0.47	0.58	0.60−0.65
Rb^+	1.5	4.0	0.65	0.64	0.66−0.69
Ca^{2+}	1.0	3.6	0.05	0.39	0.53−0.57
Sr^{2+}	1.2	3.8	0.14	0.42	0.53−0.59

for typical supercritical states. As water becomes much less dense, the decrease in τ for water about water is more substantial than for the case of water about ions, an observation consistent with the average coordination numbers. Because the ion−water interactions are still quite strong, these coordination numbers at 673 K and 0.087 g/cm^3 for water about ions are not reduced far below the values in AW.[8] In contrast, the loss in the first shell for pure water is much more pronounced due to the relatively weaker water−water interactions.

Walden Product. We are now in a position to examine the manner in which the forces evident in the solvent reorientation times are reflected in transport properties. We first examine the Walden product and the effective Stokes−Einstein radius.

An empirical rule suggests that the Walden product (conductivity times viscosity) is inversely proportional to the ionic radius, for infinitely dilute ionic solutions at constant temperature. Combining eqs 10, 11, and 12 yields the result $\Lambda_o\eta = Fe/(\sigma\pi R_{eff})$. As shown by eq 11, for the present model, the effective Stokes radius R_{eff} is a constant in the case where $\tau^R_{bulk}/\tau^R_{ion}$ is constant. Deviations from this ideal constant behavior for Walden products have been widely discussed by experimentalists and theoreticians.[36,37]

Table 5 shows the values of Walden products of ions in AW, evaluated with $\sigma = 4$, as in earlier work.[14] Also given are the radii of the ion and complex, R_I and R_C, respectively, calculated on the basis of the MD ion−water pair distribution functions. The choice of R_C follows the formulation of ref 14 and utilizes the fact that the outermost atom in the first shell of an anion or a cation is a hydrogen atom although the water orientations are different. For a cation, a most probable outer distance (D) is defined by the position of the first peak in $g_{IH}(r)$ and for an anion by the position of the second $g_{IH}(r)$ peak. The value of R_C is obtained by adding the radius of a hydrogen atom (0.5 Å) to the distance D. On the other hand, R_I is calculated for an anion from the position of the first peak in $g_{IH}(r)$ less the radius of a hydrogen atom. For a cation, R_I results from the position of the first peak in $g_{IO}(r)$ less the radius of an oxygen atom (1.4 Å). The same values of R_I and R_C (Table 5) describing ambient conditions were also used for all other state point conditions. For the calculation of the ion TCFs given by eq 1, we considered all water molecules present in a spherical region surrounding the ion given by $r < R_C$. For bulk water, the spherical region was defined as $r < 3.5$ Å at ambient conditions and $r < 4$ Å in SCW, as determined by the minimum after the first peak in the $g_{OO}(r)$ pair correlation function for pure water.

The calculated Walden products that follow from the ratios (eq 12) are also in fairly good agreement with experimental values for monovalent ions, although apparently less so for divalent ions. This is not surprising because the second shell should play a significant role for divalent cations. We also note that for these, we found that the slower dynamics lead to relatively large uncertainties compared with the monovalent ions. Nevertheless, we report the results obtained for completeness.

Figure 1 depicts values of Walden products at sub- and supercritical conditions calculated according to eq 12 with the ratios of reorientation times listed in Tables 3 and 4. Also shown in Figure 1 are two limiting cases described by the Stokes−Einstein law with (a) viscosity in the first shell equal to bulk viscosity ($R = R_I$, bare ion radius); and (b) viscosity in the first solvent shell ≫ bulk viscosity ($R = R_C$, radius of a complex including one coordination shell). At ambient conditions, Walden products for all cations fall between those of these limiting laws. The deviation from the bare ion limit increases with decreasing radius. The trend is in good agreement with experimental data.[37] Of particular note is the fact that the range of variation of Walden products is quite small (∼0.4 to 0.6) despite the wide range in temperature, density, and viscosity. The Walden product is constructed to largely remove the effect of viscosity. The observed variation with temperature of the Walden product at subcritical temperatures that is reflected in Figure 1 is, in fact, within the uncertainty of the simulated results. Nevertheless, it is worth noting that the trends in the Walden product with temperature need not be monotonic and can vary with ionic species. This variation is the result of the fact that the temperature dependence of Λ_o and solvent viscosity oppose each other, whereas only Λ_o depends on the ionic species. The other transport properties, Λ_o, ζ, and D, all vary strongly with density because they depend directly upon viscosity.

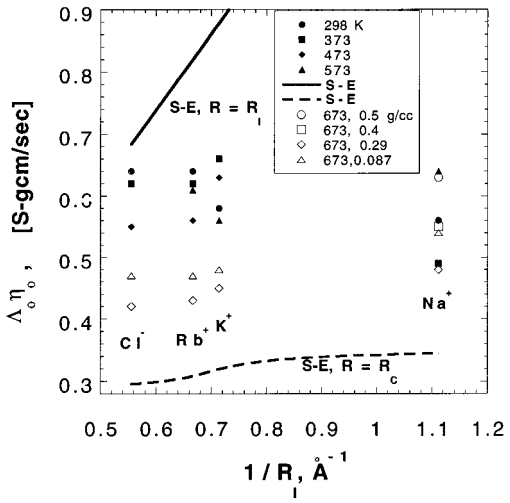

Figure 1. Walden products for ions in aqueous solution at subcritical conditions (filled symbols) along the coexistence curve of liquid water and along supercritical isochores (open symbols). (Friction coefficient evaluated using $\sigma = 4$ in eq 10.)

As already shown, the Walden product is inversely proportional to the effective Stokes radius. The effective Stokes−Einstein radius is shown in Figure 2 according to eq 11 and inferred from experiment. For a small ion such as Na^+, the effective Stokes−Einstein radius obtained from the semicontinuum model is much larger than the bare ion value, but is somewhat smaller than the Stokes−Einstein radius that was regressed from the experimental data. For Cl^-, with a smaller charge per radius, the effective Stokes−Einstein radius is closer to the bare ion limit and to the experimental value than to R_C. Here, the Stokes−Einstein equation is applicable with the bare ion radius, as has been demonstrated by experimental studies in AW for iodide[38] and other ions.[36]

In subcritical water, $\tau^R_{bulk}/\tau^R_{ion}$ is relatively constant, and thus R_{eff} and the Walden product are also similarly constant. As temperature increases and density decreases to SCW conditions, the Walden products of the ions, except for Na^+, shift toward the $r = R_c$ limit, with a larger R_{eff}. The dynamics are such that the first shell solvent is more strongly coupled to the ion. This

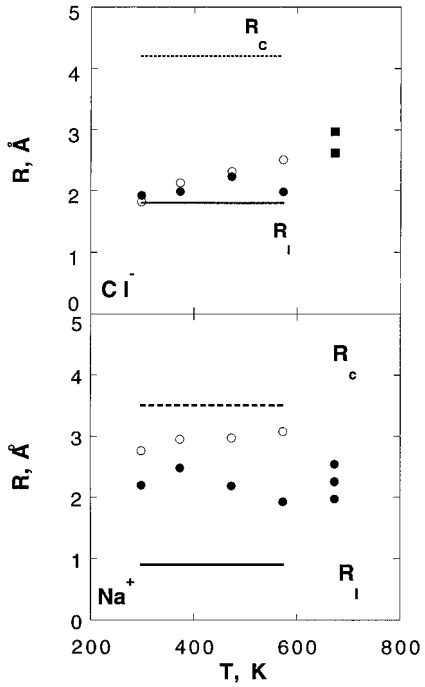

Figure 2. Effective Stokes−Einstein radii for Cl^- and Na^+ at subcritical (circles) and supercritical (squares) conditions, from calculated diffusion coefficients (filled symbols) and experimental data[40](open symbols). Also shown, the bare ion radius R_I and the radius of the complex R_C (ion + first shell) evaluated as described in the text. (Diffusion coefficients evaluated using $\sigma = 4$ in eq 10.) Cl^- at 673 K: top to bottom: 0.29 and 0.087 g/cm^3. Na^+ at 673 K: top to bottom 0.29, 0.4, 0.087 (equal), and 0.5 g/cm^3, respectively.

TABLE 6: Residual Friction (10^9 $\Delta\zeta$, poise-cm) for Ions at Sub- and Supercritical Conditions ($\sigma = 4$ in eq 10); experimental values[40] in parentheses)

		10^9 $\Delta\zeta$, poise-cm		
T, K	ρ, g/cm^3	Cl^-	Na^+	K^+
298	0.997	0.14 (−0.01)	1.45 (1.95)	0.80 (0.83)
373	0.958	0.06 (0.11)	0.56 (0.70)	0.16 (0.43)
473	0.850	0.07 (0.07)	0.22 (0.34)	0.09 (0.18)
573	0.670	0.02 (0.08)	0.11 (0.22)	0.08 (0.13)
673	0.29	0.06	0.09	0.07
673	0.087	0.03	0.04	0.04

stronger coupling reflects the reduction in counterbalancing solvent−solvent forces acting on the first shell solvent that arise at higher solvent densities from the second and further solvent layers. Thus, the net effect is a stronger ion-first shell coupling. Nevertheless, within the SCW regime, the effective Stokes radius does decrease with decreasing density due to the eventual loss of solvation.[6,8,39]

Residual Friction. The results for the Walden product may be further understood by considering that the origins of the Stokes−Einstein law include friction due only to viscous forces and ignores dielectric effects. Dielectric effects are incorporated implicitly in the effective radius and in the present semicontinuum model via the reorientation times in the first shell of the ion.

To quantify the effects of friction, it is informative to analyze a residual friction $\Delta\zeta$, defined as the difference between the total friction given by either eq 10 or experiment and that due to Stokes law for the bare ion radius. The results are presented in Table 6. At low temperatures, $\Delta\zeta$ is small for Cl^- in comparison with the other ions. Experimental values[40] of $\Delta\zeta$ are actually slightly negative for Cl^- and are small for Rb^+ (not shown) above 100 °C. The data show that as the ionic size decreases from K^+ to Na^+, the residual friction becomes increasingly more important due to the higher charge−radius ratio. The calculated values of $\Delta\zeta$ determined here are similar in magnitude to those correlated from experimental data by Oelkers and Helgeson.[40] For small ions such as Na^+, dielectric friction is comparable in magnitude to viscous friction. Similar behavior has been observed experimentally for other small ions, for example Li^+ and F^-.[36] As expected, when the ionic radius increases (e.g., in the case of Cl^-, K^+, and Rb^+), dielectric friction becomes smaller than viscous friction and in some cases can be neglected.

TABLE 7: Relative Residual Friction for Ions at Sub- and Supercritical Conditions (values independent of σ, eq 10)

		$\Delta\zeta/\zeta_{SE}$		
T, K	ρ, g/cm^3	Cl^-	Na^+	K^+
298	0.997	0.07	1.44	0.52
373	0.958	0.10	1.75	0.32
473	0.850	0.24	1.43	0.39
573	0.670	0.10	1.14	0.57
673	0.5		1.18	
673	0.4		1.51	
673	0.29	0.63	1.82	0.94
673	0.15	0.75		
673	0.087	0.45	1.50	0.82

We note that new values of residual friction coefficients for cations in ambient conditions were reported very recently.[41] These values were based on measurements of conductance at finite concentrations, extrapolated via standard models for ionic conductivity to infinite dilution. The reported $\Delta\zeta$ for Na^+, K^+, and Rb^+ agree more closely with the present calculated values than with those obtained via the Hubbard−Onsager hydrodynamic model.[18,19]

Our calculated values of $\Delta\zeta$ for ions in SCW (Table 6) indicate that residual friction is reduced ~1 order of magnitude in going from AW to typical SCW conditions. Most of this reduction takes place by 573 K because of the large decrease in bulk viscosity. At supercritical temperatures, ζ itself becomes small so that it is expected that $\Delta\zeta$ becomes small. Thus, although $\Delta\zeta$ is small, it still has a significant effect on the conductance. To see this clearly, we consider the relative residual friction, given by the ratio of the residual friction to the Stokes law friction evaluated with the bare ion radius. In Table 7, $\Delta\zeta/\zeta_{SE}$ is shown for conditions in Table 3 and additional densities in Table 4. This value is actually larger for K^+ and Cl^- in SCW than at lower temperatures, including AW. This result is consistent with local density augmentation or electrostriction of water about ions that becomes prevalent in SCW where the bulk density is small.[6] Unlike the case for the other ions, $\Delta\zeta/\zeta_{SE}$ for Na^+ is as large at low temperatures as in SCW. Nonetheless, the significant increase in $\Delta\zeta/\zeta_{SE}$ from the values at 573 K and 673 K at high densities to the results at 673 K and low densities is analogous to the results for the other ions. Eventually, as the density becomes very low (e.g., 0.087 g/cm^3), the relative residual friction decays, as does the local density, for all of the ions. As a consequence of the residual frictional forces, Walden products, diffusion coefficients and limiting conductances are significantly lower than those predicted by the Stokes−Einstein law for the bare ion.

Limiting Conductance. The limiting ionic conductance is simply related to the friction coefficient via $\Lambda_o = Fe/\zeta$. As depicted in Figure 3, the limiting ionic conductance is a steadily increasing function of temperature as friction decreases. The Stokes−Einstein equation with the bare ion radius gives this trend, but overpredicts Λ_o because it neglects residual friction.

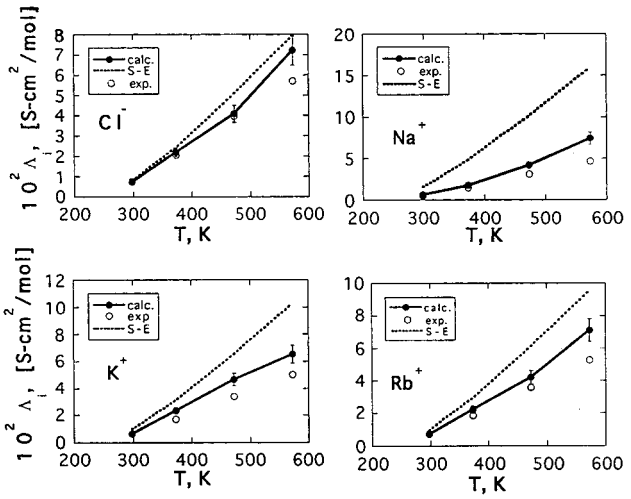

Figure 3. Limiting conductances for ions in aqueous solutions, at subcritical conditions, along the coexistence curve of water. Experimental results are from Oelkers and Helgeson[40]. (Friction coefficient evaluated using σ=4 in eq 10.)

The predictions of the semicontinuum model agree closely with experiment at low temperatures, but are modestly larger than the data at higher temperatures. We note that the uncertainty in the experimental data increases in the high-temperature region where ion association becomes prevalent and less is known about the mechanism of ion conductance. These factors complicate data reduction for determining the limiting ionic conductance. Thus, one cannot be certain in assigning these deviations to limitations of theory versus experiment.

The activation energy for conductance (or likewise diffusion) can be defined by an Arrhenius expression[42] of the form

$$\Lambda_o = AT^{-1} \exp(-E/RT) \qquad (14)$$

Because the ion diffusion coefficient is directly proportional to the product $\Lambda_o T$, E is the activation energy of the diffusion process. For NaCl in AW, the activation energy E obtained from linear regression of our calculated values from 300 to 600 K, 3.71 kcal/mol,[29] is in good agreement with the experimental value of 3.4 kcal/mol.[40] The inclusion of excess friction is essential for this good agreement. In SCW at constant density, the activation energies are much smaller, on the order of <1 kcal/mol. The small barrier is consistent with the much smaller friction resulting in part from a smaller viscosity.

In SCW, we performed additional calculations for Na^+ and Cl^- at some of the near-critical conditions at 280 bar that were studied experimentally.[2] These points are labeled with an asterisk in Table 4. Because the model critical properties differ from the experimental ones, the simulations were done at the same reduced conditions (tabulated). The experimental densities were calculated from the NIST equation of state[27] at 280 bar. The proximity to the critical point makes both the experiments and simulations challenging. Simulation runs of at least 200 ps were performed at each of these points. The effects of even longer runs or the finite size of the system on the simulation results cannot be estimated at this time.

The model predicts higher limiting conductances when compared with those inferred from experiment (Figure 4). In particular, for $\sigma = 4$ in eq 10, the model values are roughly twice as large as those of Zimmerman et al.[2] With the alternative approximation putting $\sigma = 6$ in eq 10, the calculated values are much closer to experiment, although still larger. The predictions are, in any case, far better than those of the bare ion radius Stokes−Einstein equation. Again, these results illustrate the importance of residual friction in SCW.

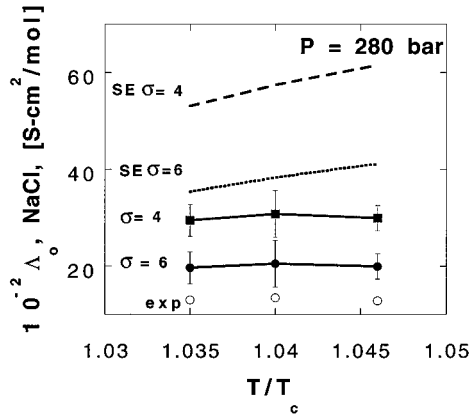

Figure 4. Limiting conductances for NaCl in aqueous solution, supercritical conditions, along the 280 bar isobar. Experimental results are from Zimmerman *et al.*[2]

The experiments already cited by Zimmerman et al.[2] are based on an advanced conductivity cell capable of studying much more dilute solutions than measured previously and also lower solvent densities. Access to such low salt concentrations enhance the expected reliability of theoretical models used to interpret the finite concentration data and extract limiting conductances and association constants. However, the implications developed from earlier experimental measurements[1] and those from these new studies are not in agreement for estimated values of limiting conductances at solvent densities lower than ~0.5 g/cm^3 (Figure 5). We note that the limiting conductance is relatively insensitive to temperature in the supercritical region.[1,2] Hence, correlations that are only functions of solvent density, corresponding to the representations used for experimental data[1,2] are given here. The results can be summarized by two alternative trends. First, for the earlier data of Quist and Marshall,[1] which were extrapolated to infinite dilution from relatively higher concentration, the limiting conductance increases approximately linearly with decreasing solvent density. On the other hand, the results of Zimmerman et al.[2] (triangles) appear to reach a plateau value at <0.5 g/cm^3. Both sets are included in Figure 5 along with our calculated values (circles). As was seen in relation to Figure 4, the calculated results evaluated with $\sigma = 6$ in eqs 3 and 10 are closer to experiment than are those evaluated with $\sigma = 4$.

Additional results for the semicontinuum and bare ion radius Stokes−Einstein models are shown for the Na^+ and Cl^- ions in Figure 6. The model results follow the extrapolation of Quist and Marshall[1] in that they are fairly linear in density and do no exhibit the plateau behavior seen by Zimmerman *et al.*[2] According to the Stokes−Einstein model, friction decreases toward zero as the density and viscosity approach zero; additional contributions associated with changes in residual friction are not predicted to produce a plateau in Λ_o, according to the semicontinuum model over the range studied here.

Conclusions

The molecular data based on simulated solvent rotational reorientation provide a route to insight into the dynamics of ion transport as well as quantitative estimates of the friction coefficient. Along the coexistence curve of water, the ratio of the rotational reorientation time for bulk water to that of water about the various ions, $\tau^R_{bulk}/\tau^R_{ion}$, is relatively constant. Consequently, the Walden product, effective Stokes−Einstein radius,

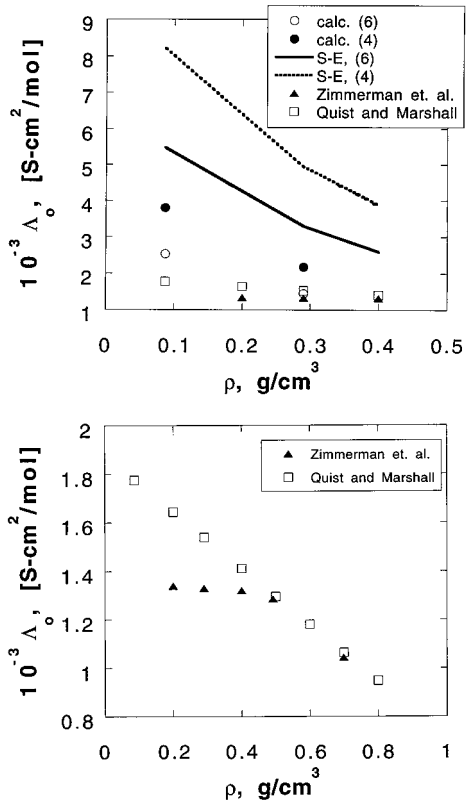

Figure 5. Limiting equivalent conductance for NaCl at 673 K calculated via semicontinuum model and via Stokes−Einstein relation compared with experimental data of Zimmerman et al.[2] and of Quist and Marshall[1]. Upper panel shows experimental data on an expanded scale at low solvent density. The values of 4 and 6 in the legend refer to σ.

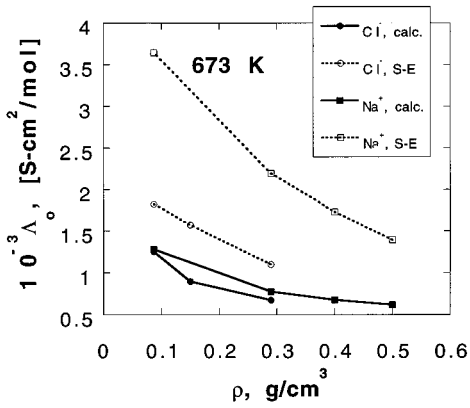

Figure 6. Limiting equivalent conductances (σ = 6 in eq 3) for individual ions at 673 K.

and relative residual friction implied by the semicontinuum model for ion transport are also fairly constant. This small change in $\tau^R_{bulk}/\tau^R_{ion}$ along the coexistence curve is a result of a similar temperature dependence for rotational dynamics for the pure solvent and the solvent associated with ions over this relatively high solvent density regime.

As the temperature is increased above the critical point, various changes are observed for densities ≤0.29 g/cm^3. The bulk solvent reorientation times decrease more quickly than those for water about an ion, a result of the relatively stronger ion−water interactions compared with water−water interactions. Correspondingly, the local viscosity in the ionic solvation shell remains larger than that in the bulk solvent, with the result that the effective Stokes−Einstein radius increases for the larger ions and the relative residual friction increases, compared with higher densities, for all of the ions. Alternatively, one can rationalize the fact that the first shell is more coupled to the ion at supercritical conditions via increasing electrostriction, the large solvent density augmentation about ions compared with the decreasing bulk density. Of course, at a given temperature in SCW, the effective Stokes−Einstein radius does decrease as the density is decreased, due to desolvation, as is also reflected in the average coordination numbers.

Our semicontinuum model yields results in reasonably good agreement with experiment at temperatures up to 400 K, but predicts larger limiting conductances than experiment at higher temperatures for NaCl. In SCW, the calculated values for limiting conductance agree best with experiments when an approximation yielding a higher friction coefficient is used (σ = 6), suggesting that the relative residual friction is enhanced in SCW compared with subcritical water. We find that changes in residual friction in the SCW regime do not appear to produce a plateau in Λ_o because solvent density is lowered over the range studied. Our results parallel more closely the linear increase in limiting ionic conductance inferred by Quist and Marshall[1] and Ho et al.,[43] rather than the plateau inferred by Zimmerman et al.[2]

The theoretical model used here includes a number of approximate elements that might contribute to the disagreements with experiment. These elements include the underlying intermolecular potentials used, as well as the parameters and formulation of the semicontinuum model. Nevertheless, the completely independently evaluated trends seen here as a function of solvent density do correspond to a simple monotonic extrapolation, which is in accord with a particular subset of the experimental analyses available. This observation certainly provides considerable motivation for further theoretical work as well as for a reexamination of the assumptions underlying the analysis of the experimental data, so that one can enhance the ability to determine limiting conductances and association equilibrium constants from conductivity data at finite concentration.

Acknowledgment. We gratefully acknowledge support from the Department of Energy (DE-FG07-96ER14687). We are also grateful for additional support from the U.S. Army for a University Research Initiative Grant (30374-CH-URI) and an AASERT grant (DAAH 04-95-1-0649, as well as from the R. A. Welch Foundation, and the Separations Research Program at the University of Texas, a consortium of over 30 companies.

References and Notes

(1) Quist, A. S.; Marshall, W. L. *J. Phys. Chem.* **1968**, *72*, 684−703.
(2) Zimmerman, G. H.; Gruszkiewicz, M. S.; Wood, R. H. *J. Phys. Chem.* **1995**, *99*, 11612−11625.
(3) Lamb, W. J.; Hoffman, G. A.; Jonas, J. *J. Chem. Phys.* **1981**, *74*, 6875−6880.
(4) Flarsheim, W. M.; Tsou, Y. M.; Trachtenberg, I.; Johnston, K. P.; Bard, A. J. *J. Phys. Chem.* **1986**, *90*, 3857.
(5) Butenhoff, T. J.; Goemans, M. G. E.; Buelow, S. J. *J. Phys. Chem.* **1996**, *100*, 5982−5992.
(6) Flanagin, L. W.; Balbuena, P. B.; Johnston, K. P.; Rossky, P. J. *J. Phys. Chem.* **1995**, *99*, 5196−5205.
(7) Flanagin, L. W.; Balbuena, P. B.; Johnston, K. P.; Rossky, P. J. *J. Phys. Chem.* **1997**, *101*, 7798−8005.
(8) Balbuena, P. B.; Johnston, K. P.; Rossky, P. J. *J. Phys. Chem.* **1996**, *100*, 2706−2716.
(9) Luo, H.; Tucker, S. C. *J. Am. Chem. Soc.* **1995**, *117*, 11359−11360.
(10) Balbuena, P. B.; Johnston, K. P.; Rossky, P. J. *J. Phys. Chem.* **1996**, *100*, 2716−2722.
(11) Cui, S. T.; Harris, J. G. *Chem. Eng. Sci.* **1994**, *49*, 2749−2763.

(12) Kalinichev, A. G. *Ber. Bunsen-Ges. Phys. Chem.* **1993**, *97*, 872−876.
(13) Mountain, R. D.; Wallqvist, A. "A Collection of Results for the SPC/E Water Model," NIST, 1996.
(14) Impey, R. W.; Madden, P. A.; McDonald, I. R. *J. Phys. Chem.* **1983**, *87*, 5071−5083.
(15) Bird, R. B.; Stewart, W. E.; Lightfoot, E. N. *Transport Phenomena*; J. Wiley & Sons: New York, 1960.
(16) Brilliantov, N. V.; Krapivsky, P. L. *J. Phys. Chem.* **1991**, *95*, 6055−6057.
(17) Wolynes, P. G. *Annu. Rev. Phys. Chem.* **1980**, *31*, 345−376.
(18) Hubbard, J.; Onsager, L. *J. Chem. Phys.* **1977**, *67*, 4850−4857.
(19) Hubbard, J. B. *J. Chem. Phys.* **1978**, *68*, 1649−1664.
(20) Jonas, J.; DeFries, T.; Wilbur, D. J. *J. Chem. Phys.* **1976**, *65*, 582−588.
(21) Hansen, J.-P.; McDonald, I. R. *Theory of Simple Liquids;* 2nd. ed.; Academic: San Diego, CA, 1990.
(22) Zichi, D. A.; Rossky, P. J. *J. Chem. Phys.* **1986**, *84*, 2814−2822.
(23) Berendsen, H. J. C.; Grigera, J. R.; Straatsma, T. P. *J. Phys. Chem.* **1987**, *91*, 6269−6271.
(24) Belhadj, M.; Alper, H. E.; Levy, R. M. *Chem. Phys. Lett.* **1991**, *179*, 13−20.
(25) de Leeuw, S. W.; Perram, J. W.; Smith, E. R. *Proc. R. Soc. London* **1980**, *A 373*, 27−56.
(26) Guissani, Y.; Guillot, B. *J. Chem. Phys.* **1993**, *98*, 8221−8235.
(27) Gallagher, J. S.; Haar, L. In *U. S. National Bureau of Standards*; Nat. Eng. Lab., Thermophysics Division: Gaithersburg, Maryland, 1985.
(28) Ladanyi, B. M.; Skaf, M. S. *Annu. Rev. Phys. Chem.* **1993**, *44*, 335−368.
(29) Balbuena, P. B. Ph.D. Thesis, University of Texas at Austin, 1996.
(30) Neumann, M. In *Physical Chemistry of Aqueous Systems: Meeting the Needs of Industry*; White, H. J., Jr., Ed.; Begell House: New York, 1995; pp 261−268.
(31) vanGunsteren, W. F.; Berendsen, H. J. C.; Rullmann, J. A. C. *Far. Discuss.* **1978**, *66*, 58−69.
(32) Postorino, P.; Tromp, R. H.; Ricci, M.-A.; Soper, A. K.; Neilson, G. W. *Nature* **1993**, *366*, 668−670.
(33) Mizan, T. I.; Savage, P. E.; Ziff, R. M. *J. Phys. Chem.* **1995**, *100*, 403−408.
(34) Endom, L.; Hertz, H. G.; Thul, B.; Zeidler, M. D. *Ber. Bunsen-Ges. Phys. Chem.* **1967**, *71*, 1008−1031.
(35) Engel, G.; Hertz, H. G. *Ber. Bunsen-Ges. Phys. Chem.* **1968**, *72*, 808−834.
(36) Smedley, S. I. *The Interpretation of Ionic Conductivity in Liquids*; Plenum Press: New York, 1980.
(37) Evans, D. F.; Tominaga, T.; Hubbard, J. B.; Wolynes, P. G. *J. Phys. Chem.* **1979**, *83*, 2669−2677.
(38) Flarsheim, W. M.; Bard, A. J.; Johnston, K. P. *J. Phys. Chem.* **1989**, *93*, 4234.
(39) Balbuena, P. B.; Johnston, K. P.; Rossky, P. J. *J. Phys. Chem.* **1995**, *99*, 1554−1565.
(40) Oelkers, E. H.; Helgeson, H. C. *J. Sol. Chem.* **1989**, *18*, 601−640.
(41) Ueno, M.; Tsuchihashi, N.; Yoshida, K.; Ibuki, K. *J. Chem. Phys.* **1996**, *105*, 3662−3670.
(42) Oelkers, E. H.; Helgeson, H. C. *Geochim. Cosmochim. Acta* **1988**, *52*, 63−85.
(43) Ho, P. C.; Palmer, D. A.; Mesmer, R. E. *J. Sol. Chem.* **1994**, *23*, 997−1018.
(44) Robinson, R. A.; Stokes, R. H. *Electrolyte Solutions*; Butterworth Scientific Publications: London, 1959.